Chinese Chemical Letters 37 (2026) 112105

Contents lists available at ScienceDirect

Chinese Chemical Letters

journal homepage: www.elsevier.com/locate/cclet

Supramolecularly engineered bacteria reactors mediated cyclic consumption of lactic acid for targeted cancer therapy

Xun Xu[a,1], Jianwen Wei[a,1], Yuan-Fu Ding[b,*], Junyan Li[a], Mian Tang[a], Chun Wang[c], Beibei Xie[a], Qingwen Zhang[a,*], Yan Gao[a,*]

[a] State Key Laboratory of Mechanism and Quality of Chinese Medicine, Institute of Chinese Medical Sciences, University of Macau, Macau 999078, China
[b] School of Medical and Information Engineering, Gannan Medical University, Ganzhou 341000, China
[c] College of Biology and Food Engineering, Guangdong University of Petrochemical Technology, Maoming 525024, China

ARTICLE INFO

Article history:
Received 8 July 2025
Revised 31 October 2025
Accepted 11 November 2025
Available online 12 November 2025

Keywords:
Supramolecularly engineered bacteria
Cancer metabolic treatment
Cyclic lactic acid consumption
Tumor colonization
Targeted accumulation

ABSTRACT

Lactic acid plays a crucial role in tumor growth, maintenance, and metastasis. Given its significant impact on tumorigenesis, modulating lactic acid levels within the tumor microenvironment (TME) presents new opportunities for cancer therapy. Herein we developed a supramolecularly engineered bacterial reactor using a strong host-guest interaction between cucurbit[7]uril (CB[7])-modified attenuated *Salmonella typhimurium* VNP20009 (VNP) and adamantane (ADA)-functionalized lactate oxidase (LOX)-loaded liposomes. The VNP-mediated tumor colonization of these reactors facilitated LOX-driven lactic acid depletion in the hypoxic TME, simultaneously producing hydrogen peroxide (H_2O_2). The presence of H_2O_2 triggered the expression of catalase in VNP, which, in turn, catalyzed the conversion of H_2O_2 to oxygen (O_2). This cyclic cascade reactor thus provided a continuous and stable oxygen source, promoting sustained lactic acid consumption for metabolic treatment, ultimately leading to tumor growth suppression and an enhanced anticancer effect.

© 2026 Published by Elsevier B.V. on behalf of Chinese Chemical Society and Institute of Materia Medica, Chinese Academy of Medical Sciences.

The pathological tumor microenvironment (TME) includes carcinoma cells, mesenchymal cells, and immune cells, and manifests as abnormal vasculogenesis, hypoxia, and acidity [1–3]. In the hypoxic TME, tumor cells produce large amounts of lactic acid *via* aerobic glycolysis [4]. Lactic acid is closely associated with tumorigenesis, serving not only as a substrate to provide energy to tumor cells but also as a signaling molecule that activates various pathways to promote tumor cell invasion, metastasis, angiogenesis, and immune escape [5–10]. Recent discoveries indicate that lactic acid suppresses the expression of the macrophage-specific vacuolar ATPase subunit and enhances hypoxia-inducible factor 2α (HIF-2α)–mediated vascular endothelial growth factor (VEGF) production in the TME [11]. Current research focuses on inhibiting key enzymes and monocarboxylate transporters in the glycolytic process [12–14]. However, the low bioavailability and potential systemic toxicity of glycolysis inhibitors necessitate the development of novel methods targeting lactic acid metabolism for cancer treatment. One emerging approach involves the direct consumption of intracellular and extracellular lactic acid using lactate oxidase (LOX) [15]. LOX catalyzes the aerobic oxidation of lactic acid to pyruvate, producing H_2O_2 in the process [16]. This reaction decreases the levels of lactic acid and O_2 while increasing the concentration of H_2O_2. Numerous studies have demonstrated the potential of LOX in cancer treatment [17–19]. For instance, Dai *et al.* developed a metal-phenolic network-based nano-complex that loads LOX and the mitochondrial respiration inhibitor atovaquone to remodel the immunosuppressive TME [20]. Zhang *et al.* constructed a cell membrane-coated hollow MnO_2 catalytic nano-system embedded with LOX and a glycolysis inhibitor for synergistic metabolic therapy [21]. Recently, Hong *et al.* encapsulated L-arginine and LOX into hollow MnO_2 nanoparticles to reverse tumor immunosuppression and sensitize immune checkpoint blockade therapy [22]. In spite of all these preliminary successes, the large consumption of oxygen by LOX in the already hypoxic environment can lead to high deficiency of oxygen, which limits the efficiency of LOX catalysis and exacerbates hypoxia in the TME [23].

In recent years, bacteria-based therapeutic systems have garnered significant interest, particularly for cancer therapy. Anaerobic and facultative anaerobic bacteria have shown high selectivity and the ability to deeply colonize hypoxic tumor tissues [24–26]. Bacterial colonization in the tumor sites can compete with cancer

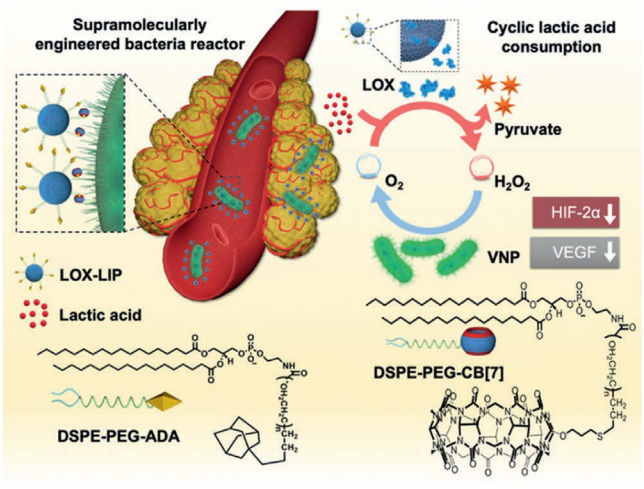
* Corresponding authors.
E-mail addresses: yfding@gmu.edu.cn (Y.-F. Ding), qwzhang@um.edu.mo (Q. Zhang), gaoyanki@hotmail.com (Y. Gao).
[1] These authors contributed equally to this work.

https://doi.org/10.1016/j.cclet.2025.112105
1001-8417/© 2026 Published by Elsevier B.V. on behalf of Chinese Chemical Society and Institute of Materia Medica, Chinese Academy of Medical Sciences.

cells for nutrients in the TME, thus limiting tumor growth [27]. Additionally, the inherent pro-inflammatory capacity of bacteria can stimulate the body's immune system [28]. Therefore, developing bacterial delivery systems to achieve enhanced anti-tumor effects could potentially become a promising cancer therapeutic strategy [29]. *Salmonella* is a group of intracellularly invasive Gram-negative facultative anaerobic bacteria that can survive in both aerobic and anaerobic environments [30]. VNP20009 (VNP) is a well-studied clinical strain of attenuated *Salmonella typhimurium* that has demonstrated high tumor targeting and safety in Phase I clinical trials [31]. Zheng *et al*. injected tumor-bearing mice with VNP and found that bacterial accumulation at tumor sites was 200–1000 times greater than at other normal tissues, resulting in significantly delayed tumor growth [32]. Meanwhile, exposure to oxidative damage conditions *in vivo* activates a variety of proteins in bacteria to respond to harmful oxidants [33,34]. *S. typhimurium*, for instance, overexpresses several enzymes, including catalase, to combat H_2O_2-induced oxidative stress [35,36]. Due to their preferential and selective accumulation in tumor tissues and catalase-like properties, bacterial delivery systems offer a potential opportunity for the precise and persistent modulation of lactic acid levels in the TME.

Supramolecular host-guest interaction has shown considerable promise in the field of drug delivery systems including live bacterial-drug delivery systems. For the conjugation of drug cargo onto the surface of bacterial, host-guest interaction significantly reduce the complexity and reaction time of chemical covalent conjugation by employing a facile, general, and bioorthogonal method between host-guest pairs such as cucurbit[7]uril (CB[7]) and adamantane (ADA) pair with a short reaction time (serval minutes) and high binding affinity ($K_a > 10^6$ L/mol), which providing a more specific bonding and a stronger force than physical factors like electrostatic interaction, hydrophobic interaction and biological techniques like biotin-streptavidin conjugation [37–39].

Herein, we designed a bacterial reactor by supramolecularly integrating VNP20009 (VNP) and LOX-loaded liposomes (LIP) to achieve cyclic lactic acid consumption for targeted metabolic treatment of tumors (Scheme 1). VNP, a Gram-negative bacterium, has an outer membrane composed of phospholipids and proteins forming a bilayer similar to other biological membranes, facilitating surface functionalization *via* lipid insertion [40,41]. Specifically, cucurbit[7]uril (CB[7])-modified 1,2-distearoyl-*sn*–glycero-3-phosphoethanolamine-poly(ethylene glycol) (DSPE-PEG-CB[7]) ligand was inserted into the VNP outer membrane *via* lipid interactions. Adamantane (ADA)-modified LOX-loaded LIP can be facilely conjugated with VNP through strong host-guest interactions between CB[7] and ADA. The resulting supramolecular conjugate of CB[7]-modified VNP (CB[7]-VNP) and LIP exhibited tumor-targeting and accumulation capabilities due to VNP's tumor tropism towards the tumor tissues. Upon colonizing the tumor sites, the VNP is stimulated by the excess H_2O_2 in the tumor to generate O_2, consuming the H_2O_2 in the process. The produced O_2 is further supplied to the LOX loaded in LIP to catalyze the conversion of lactic acid in the TME into pyruvate and H_2O_2, creating a VNP-LOX catalytic reaction cycle. This bacterial system acts as a lactic acid depletion reactor, accelerating lactic acid catabolism. Moreover, the metabolism of lactic acid limits the expression of HIF-2α and reduces the production of the pro-tumoral factor VEGF, further inhibiting tumor vascularization and growth [11,42]. Therefore, supramolecularly integrating VNP and lactic acid-modulating LIP into a cyclic catalytic reactor can remodel the pathological microenvironment and significantly enhance the inhibition of tumor growth.



Scheme 1. Scheme showing the supramolecularly engineered bacteria conjugate (VNP-LIP) acts as a catalase-LOX cyclic catalytic reactor, derived from DSPE-PEG-CB[7] modified VNP (CB[7]-VNP) and LOX-loaded liposomes (LIP) with the ability to modulate the TME and inhibit the tumor growth.

First, we evaluated the catalase activity of VNP by quantifying oxygen production following H_2O_2 catalysis (Fig. 1A). VNP was mixed with different concentrations of H_2O_2 solution to measure oxygen production every minute. VNP was shown to catalyze H_2O_2 to produce O_2 with a dose-dependent trend. Subsequently, after treating with different concentration of H_2O_2, VNP was lysed and tested for catalase activity using a kit (Fig. 1B). The results showed that the activity of several groups pretreated with H_2O_2 was higher than that of the group without pretreatment, which reached best enzyme activity in the 50 μmol/L of H_2O_2. The higher the concentration of pretreated H_2O_2, the greater the enzyme activity. The upregulation of catalase expression started 2 h after the addition of H_2O_2, reached a peak at 6 h, and decreased until 10 h after testing (Fig. S1A in Supporting information). VNP was exposed to high concentrations of H_2O_2 during oxidative stress. To ensure the survival of VNP during this process, we performed bacterial survival experiments at different concentrations of H_2O_2. VNP was incubated in 0, 20, 50, and 100 μmol/L H_2O_2 solution for 1 h at 37 °C, diluted in PBS and plated on solid LB agar plates, and the number of colonies was counted. It was found that these selected culture concentrations did not have much impact on bacterial survival (Fig. S1B in Supporting information). After the first treatment with different concentrations of H_2O_2, VNP was treated with 100 μmol/L H_2O_2 again to see whether VNP could resist the second damage of H_2O_2. The results this time still showed the excellent resistance of VNP to high concentrations of H_2O_2 (Fig. S1C in Supporting information). In addition, as the concentration of the first round of H_2O_2 pretreatment increased, the bacterial proliferation ability also increased. The oxygen production capacity of H_2O_2-pretreated VNP was also evaluated, and 400 μmol/L was selected as the catalytic concentration of H_2O_2 (Fig. S1D). These experimental results confirmed that H_2O_2-induced oxidative stress in VNP caused increased catalase activity and oxygen production. The identification of bacterial oxidative stress provided the basis for the use of VNP with catalase activity as catalytic reactors capable of producing oxygen.

The decoration of CB[7] on the surface of VNP was achieved using 1,2-distearoyl-*sn*–glycero-3-phosphoethanolamine-poly(ethylene glycol) (DSPE-PEG) which is a lipid molecule widely used for membrane insertion [43,44]. Due to the presence of bacterial fimbriae on the surface of VNP, too short a DSPE-PEG chain length inserted into the outer membrane would interfere with the binding of CB[7] at the end of the molecule to the guest molecule [45]. Therefore, we selected DSPE-PEG with a PEG molecular weight of 5000 with a longer chain length for further synthesis. According to the previously reported methods, DSPE-PEG-CB[7] was synthesized through the thio-lene click reaction

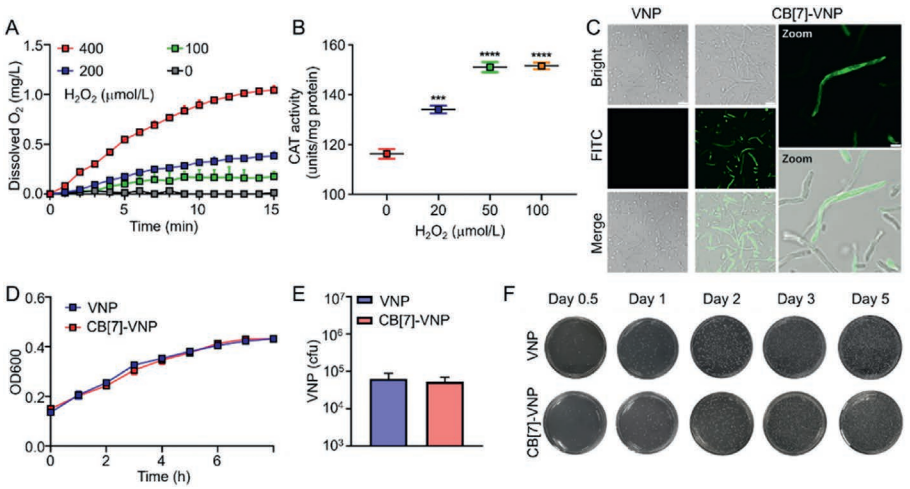


Fig. 1. (A) VNP catalyzed the production of O_2 from H_2O_2 at different concentrations. $n = 3$. (B) The relative catalase activity of VNP after treatment with different concentrations of H_2O_2, as indicated. $n = 3$. (C) VNP was incubated with PBS containing 100 μmol/L DSPE-PEG-CB[7] for 6 h. VNP without modification of DSPE-PEG-CB[7] was the control group. ADA-FITC was then added to the medium and CB[7]-VNP was imaged by CLSM after 5 min of incubation. Scale bar = 7.5 μm (2.5 μm, enlarged images). (D) Growth curve of VNP and CB[7]-VNP *in vitro*. $n = 3$. (E) The replicative capacity of VNP and CB[7]-VNP in RAW264.7 cells. $n = 3$. (F) Representative photographs of solid LB agar plates of VNP and CB[7]-VNP colonization in the tumor at 12 h, 1 d, 2 d, 3 d, and 5 d. The dilutions ratio was 1/100, 1/100, 1/100, 1/100, and 1/1000, respectively.

between monoallyloxy CB[7] and DSPE-PEG-SH and the chemical structure was confirmed by ^{1}H NMR and FT-IR spectra (Fig. S2 in Supporting information) [41]. To obtain CB[7]-VNP, VNP was first cultured in liquid LB medium overnight and then incubated with 100 μmol/L DSPE-PEG-CB[7] in PBS for 6 h. To verify the successful insertion of DSPE-PEG-CB[7], fluorescein isothiocyanate modified ADA (ADA-FITC) was used to label CB[7] on the bacterial surface *via* the CB[7]-ADA host-guest interaction. CB[7]-VNP was incubated with ADA-FITC for 5 min and then imaged by confocal laser scanning microscopy (CLSM). Confocal images confirmed the binding of ADA-FITC to CB[7]-VNP, indicating the presence of CB[7] on the bacterial surface (Fig. 1C). In contrast, almost no fluorescent FITC was detected on the VNP surface without pre-incubation with DSPE-PEG-CB[7]. Based on the high affinity of CB[7]-oxaliplatin (OX) host-guest interaction, the CB[7]-VNP was incubated with OX. After washing the free OX, Inductively Coupled Plasma-Mass Spectrometry (ICP-MS) measured the Pt content to quantify the number of CB[7] on the surface of VNP, approximately 3.9×10^{-7} nmol CB[7] per bacterium. We then examined the stability of the DSPE-PEG-CB[7] insertion. CB[7]-VNP was stored in PBS for 2, 6, 16, 24, 48, and 72 h and then incubated with ADA-FITC for 5 min. CLSM imaging detected strong green fluorescence from 2 h to 24 h, gradually weakening from 48 h to 72 h, indicating that most DSPE-PEG-CB[7] were stably modified on the bacterial surface for at least 48 h (Fig. S3 in Supporting information). This was also consistent with the results of ICP-MS quantification (Fig. S4 in Supporting information).

Then, we compared the characteristics of the VNP before and after the CB[7] modification to study whether the insertion of DSPE-PEG-CB[7] affected the activity of bacteria. We cultured unmodified VNP and CB[7]-VNP under the same condition and recorded the growth curve by measuring the optical density at 600 nm (Fig. 1D). It was found that the growth trends of both were similar, thus the insertion of the membrane did not affect bacterial proliferation. CT26 tumor-bearing female BALB/c mice were injected intravenously with unmodified VNP and CB[7]-VNP at a dose of 10^5 CFU and were sacrificed 12 h, 1 d, 2 d, 3 d, and 5 d after injection. The collected tumor tissues were homogenized, diluted with PBS, and plated on LB plates. Counting the number of colonies in each plate, the results showed that colonies in tumors injected with modified or unmodified VNP both increased exponentially over time (Fig. 1F). This suggested that the properties of anaerobic VNP that selectively colonized the hypoxic, immunosuppressed, and biochemically unique TME, were retained after CB[7] modification [46,47]. A similar amount of intracellular bacteria was observed in RAW264.7 cells, indicating that DSPE-PEG-CB[7] did not impede bacterial replication (Fig. 1E). The above experiments demonstrated that we had successfully inserted DSPE-PEG-CB[7] into the bacterial outer membrane and that this insertion had no impact on the ability of the VNP to proliferate, intracellularly replicate, and target tumors.

Since the membrane modification of DSPE-PEG-CB[7] was relatively stable, it was suitable for the preparation of VNP-LIP and subsequent targeted delivery *in vivo*. DSPE-PEG-ADA was synthesized according to previous methods [41], and the chemical structure was determined by ^{1}H NMR and FT-IR spectra (Fig. S5 in Supporting information). The LIP was prepared using lecithin, cholesterol, DSPE-PEG-ADA, and LOX by the film dispersion method [48]. The encapsulation efficiency and loading efficiency of LOX was determined to be 32.5 % and 77 %, respectively *via* BCA protein assay. The liposome diameter was measured to be 182 nm by dynamic light scattering (DLS). In addition, by loading LOX into liposomes, the degradation of LOX by bacterial proteolytic enzymes was largely avoided, effectively retaining the activity of LOX (Fig. S6 in Supporting information). The CB[7]-ADA host-guest interaction between CB[7]-VNP and LIP resulted in the formation of VNP-LIP. The morphology of VNP and VNP-LIP was observed by SEM (Figs. 2A and B). The results showed a number of distinct protruding spheres like-liposomes on the surface of VNP-LIP, while the smooth surface of VNP without pretreatment with DSPE-PEG-CB[7]. As shown in Fig. 2C, the modification of CB[7] and the binding of CB[7]-VNP with LIP both change the zeta potential of VNP, both showing negative surface charges. Similarly, we examined the growth curves of VNP and VNP-LIP, and the results showed that the conjugation of LIP had less effect on bacterial proliferation (Fig. 2D). Next, we tested the ability of the VNP-LIP to metabolize lactic acid *in vitro*. After incubating LIP, CB[7]-VNP, and VNP-LIP in the lactic acid solution for 10 min, the lactic acid concentration was detected using a kit. Compared with no change in lactic acid concentration when VNP was added alone, the significant consumption of lactic acid upon the addition of VNP-LIP indicated that the conjugated LIP had normal catalytic capacity (Fig. 2E). Since the metabolite of lactic acid catalyzed by LOX was H_2O_2, the production of H_2O_2 in solution was also studied

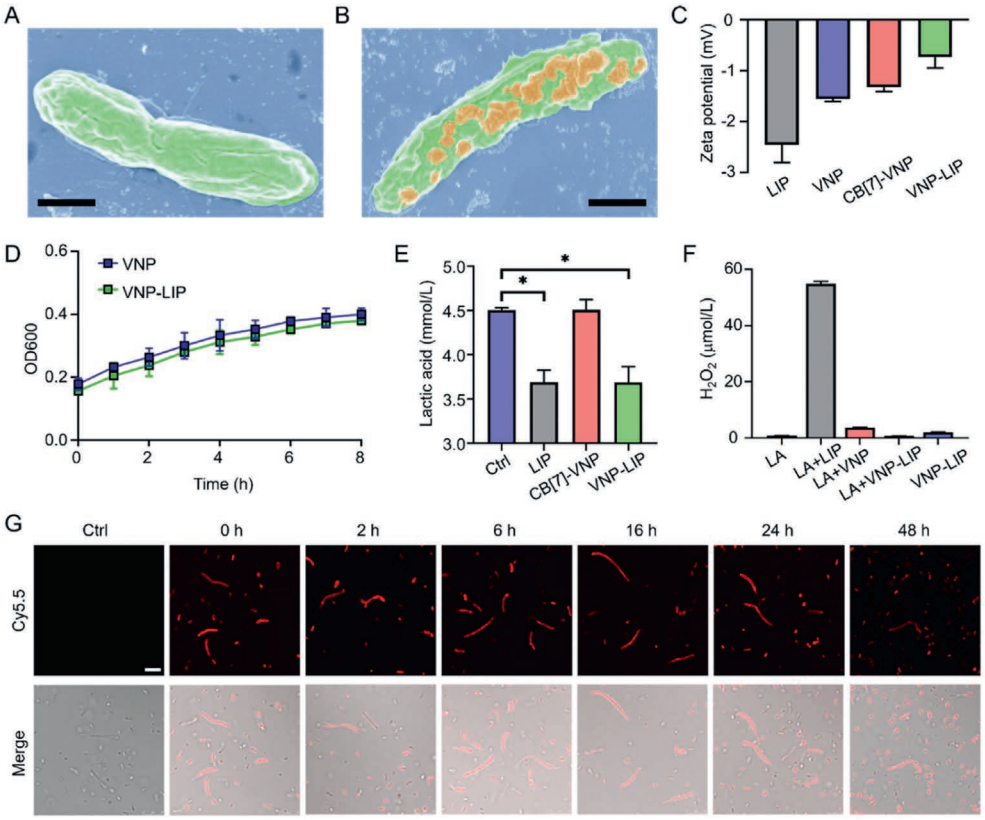


Fig. 2. (A) SEM image of VNP. Scale bar = 1 μm. (B) SEM image of the mixture of CB[7]-VNP and ADA-liposomes. Scale bar = 1 μm. (C) Zeta potential of LIP, VNP, CB[7]-VNP, and VNP-LIP. (D) Growth curve of VNP and VNP-LIP *in vitro*. $n = 3$. (E) LIP, CB[7]-VNP, and VNP-LIP mediated lactic acid consumption in lactic acid solution. $n = 3$. Data were presented as mean ± *s*.d. Statistical analysis was conducted using One-Way ANOVA. $^{*}P \leq 0.05$, $^{**}P \leq 0.01$, and $^{***}P \leq 0.001$. (F) H_2O_2 concentration in lactic acid solution after various treatments. $n = 3$. (G) The fluorescence images of Cy5.5 LIP conjugated VNP. Cy5.5 LIP conjugated VNP were incubated in PBS for 0, 2, 6, 16, 24, and 48 h, respectively. VNP without modification of DSPE-PEG-CB[7] was the control group. Scale bar = 5 μm.

(Fig. 2F). No H_2O_2 was detected in the LA group without LOX because no catalytic reaction occurred. Without adding the reaction substrate lactic acid (VNP-LIP group) or the reaction catalyst LOX (LA+VNP group), a small amount of H_2O_2 was produced probably due to the metabolism of the bacteria themselves. By using VNP with catalase property in conjunction with LOX (VNP-LIP group), the H_2O_2 produced from lactic acid catalyzed by LOX could be consumed by VNP, as evidenced by the decrease in H_2O_2 concentration in the solution. Next, we detected lactic acid consumption and O_2 production at the same time point within 10 min (Fig. S7 in Supporting information). As lactic acid was consumed, the amount of O_2 in the solution initially increased, indicating that the H_2O_2 produced by LOX metabolism was catalyzed by VNP into O_2. After that, the O_2 level plateaued, possibly because the amount of O_2 consumed by LOX and the amount of O_2 produced by VNP reached equilibrium. These results verified the successful operation of the cycle-like lactic acid-depleting reaction *in vitro*. Subsequently, Cy5.5-loaded ADA liposomes (Cy5.5-LIP) as a fluorescent tracker were incubated with CB[7]-VNP for 48 h to observe the stability of liposome binding (Fig. 2G). The intense red fluorescence was maintained for 24 h, suggesting the possibility of implementing a stable lactic acid catalytic reactor based on VNP-LIP.

Next, we investigated whether LOX enhanced the killing effect on tumor cells by activating lactic acid catabolism through the catalase activity of VNP. As shown in Figs. 3A and D, we incubated VNP-LIP with CT26 cells for 24 h and evaluated the cancer cell viability under normoxic and hypoxic conditions using a cell counting kit (CCK-8). In the presence of sufficient oxygen, LOX could consume an unlimited amount of oxygen to catalyze lactic acid decomposition, the catalytic product H_2O_2 also could induce cell apoptosis, and thus LIP exhibited stronger toxicity to CT26 cells than VNP-LIP. At only 1% oxygen content, VNP-LIP exhibited enhanced CT26 cell growth inhibition, probably because the scarcity of oxygen limited the occurrence of the LOX (LIP group) catalytic reaction, while improvement of catalytic activity due to the activated catalase-like VNP (VNP-LIP group). The reaction cycle of VNP with LIP made the oxygen supply less scarce and increased lactic acid consumption. Notably, VNP-LIP killed most tumor cells even under hypoxic conditions. The results of the lactic acid measurement in the culture medium also supported the speculation (Figs. 3B and E). At the same time, the detection of the H_2O_2 content of the catalytic product showed the increase of H_2O_2 level in the LIP group due to greater lactic acid consumption, while the decrease of H_2O_2 levels in the VNP-LIP group due to the partial conversion of H_2O_2 to O_2 by VNP, which was more evident in the hypoxic condition (Figs. 3C and F). At the cellular level, we monitored VNP-LIP mediated changes in O_2, lactic acid, and H_2O_2 levels over the same period (Fig. 3G). Over 24 h, as lactic acid in the medium continued to be depleted, O_2 levels and H_2O_2 concentrations underwent an initial sharp increase to a later leveling off. It is suggested that the engineered bacteria reactor could supply self-sufficient O_2 for catalysis, which was particularly beneficial for lactic acid metabolism in hypoxic tumor tissues.

To assess the specific tropism and colonization behavior of VNP-LIP at tumor sites, *in vivo* biodistribution assays were performed in the CT26 tumor-bearing BALB/c mouse model. When the tumor volume reached 400 mm^3, VNP-LIP was injected intravenously into CT26 tumor-bearing mice at a dose of 10^5 CFU, and major organs and tumor tissues were collected at 2, 6, 16, 24, and 48 h. The results of agar plate incubation of tissue dilutions showed that VNP

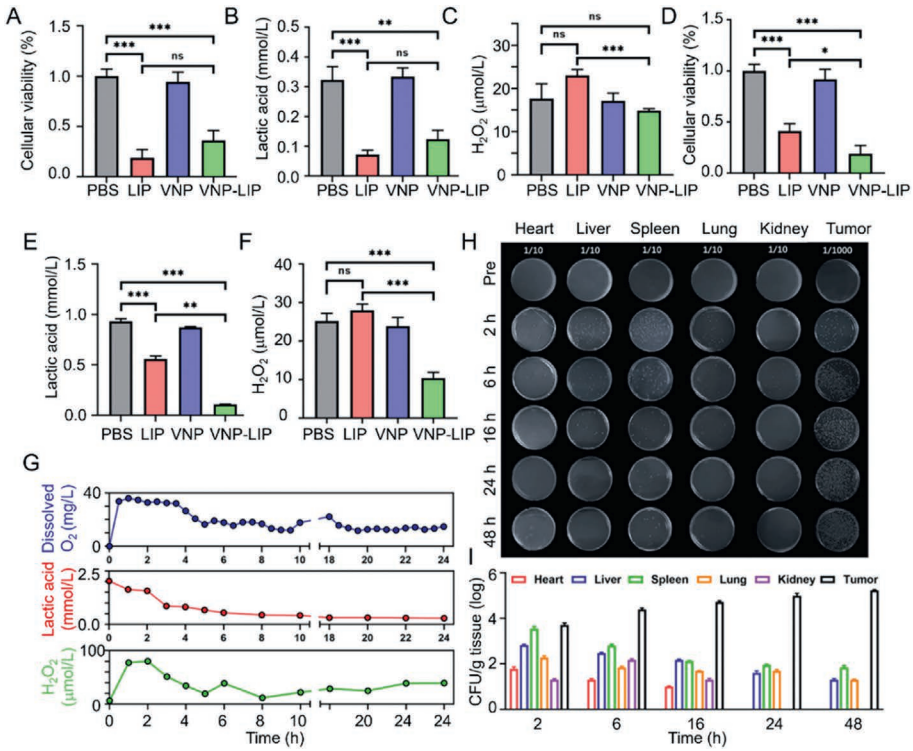


Fig. 3. (A) Cell viability, (B) cell lactic acid concentration, and (C) cell H_2O_2 production after different treatments under normoxic conditions (21 % O_2). (D) Cell viability, (E) cell lactic acid concentration, and (F) cell H_2O_2 production after different treatments under hypoxic conditions (1 % O_2). (G) Monitoring the oxygen, lactic acid, and H_2O_2 levels in CT26 cells medium within 24 h. (H) Dilutions of different organs collected from CT26 tumor-bearing mice at different time points after injection of VNP-LIP were coated on LB agar plates (H), and bacteria colonies were quantified (I). The dilution ratio was 1/10 for major organs and 1/1000 for tumors. Data were presented as mean ± *s*.d. Statistical analysis was conducted using One-Way ANOVA. $^{*}P \leq 0.05$, $^{**}P \leq 0.01$, and $^{***}P \leq 0.001$.

accumulated mainly in the tumor and was gradually eliminated from major organs in 48 h (Fig. 3H). The bacterial colony numbers in tumors were three orders of magnitude higher than other organs, indicating the excellent tumor targeting of VNP-LIP (Fig. 3I). Benefiting from the VNP-hitchhiking delivery, LIP was directly observed from frozen sections of tumor sites. Here, DiD-loaded liposomes (DiD LIP) were conjugated on the surface of VNP and acted as a red fluorescent indicator. After intravenous (i.v.) injection of DiD LIP, VNP-DiD LIP (supramolecular conjugate), and VNP+DiD LIP (physical mixture), mice were euthanized at 48 h, and tumor tissues were collected. As shown in Fig. S8 (Supporting information), lower red fluorescence was detected in the DiD LIP group and VNP+DiD LIP group, attributed to the absence of supramolecular interaction and the EPR effect of nanosized LIP. In contrast, the appearance of strong red fluorescence suggested that VNP carried DiD LIP efficiently into the tumor sites of mice in the form of VNP-LIP. In addition, bacterial colonies were counted in the major organs and peripheral blood of healthy mice after i.v. injection of VNP-LIP (10^5 CFU) at different time points (Fig. S9 in Supporting information). The results showed that no bacteria were detected in the blood at any time point, which means the bacteria were quickly cleared from the blood within 1 day. At early time points (*e.g.*, day 1 and day 3), VNP mainly accumulated in the spleen and kidneys, with numbers in other organs declining rapidly after one day. After 30 days, various organs were virtually free of bacteria, presumably due to efficient clearance by the immune system [25,32].

We investigated the potential of VNP-LIP to inhibit tumor progression using a CT26 tumor-bearing BALB/c mouse model. As shown in Fig. 4, when the tumor volume reached 100 mm^3, mice were randomly divided into four groups ($n = 6$ per group) following i.v. injection of PBS, LIP, VNP, and VNP-LIP, respectively. Monitoring of mouse body weight showed that these treatments had no significant effect on the health of the mice (Fig. 4C). Blood biochemistry and hematology analysis results within the normal range indicated that the inflammation caused by bacteria was low and tolerable for mice (Figs. S10 and S11 in Supporting information). The tumor growth curve (Fig. 4B) and the average weight of excised tumors (Fig. 4D) showed that LIP and VNP had slight therapeutic effects, while VNP-LIP had great tumor suppression potential. The tumor growth inhibition value of VNP-LIP was 71.5 %, compared to 32.6 % and 14.5 % for LIP and VNP, respectively (Fig. 4D). Compared with other groups, the administration of VNP-LIP resulted in the highest level of necrosis and apoptosis in tumor tissues, as shown by the hematoxylin and eosin (H&E) staining and the terminal deoxynucleotidyl transferase dUTP nick end labeling (TUNEL) staining of the tumor tissue sections, confirming the excellent anticancer efficacy of VNP-LIP (Fig. 4E). Due to a large amount of bacteria colonization in tumors (Fig. S12 in Supporting information), which competitively deprived cancer cells of some nutrients needed for proliferation, the VNP groups slowed tumor growth. Detection of lactic acid levels in tumor tissue of treated mice revealed the primary cause of tumor growth inhibition (Fig. 4F). Lactic acid levels were reduced in both LIP and VNP-LIP groups in comparison with the control group, suggesting that consuming lactic acid in TME by LOX played an important role in hindering cancer cell growth. With the help of tumor-tropism VNP, LOX-loaded LIP accumulated at the tumor sites, and accelerated lactic acid catabolism through the catalase-LOX reaction cycle especially in a hypoxic environment, showing better tumor suppressive effects. Moreover, accompanied by the decomposition of lactic acid, VNP-LIP markedly inhibited the expression of transcription factor HIF-2α that mediated the production of VEGF (Fig. 4G), which decreased the level of VEGF related to tumor expansion and abnormal

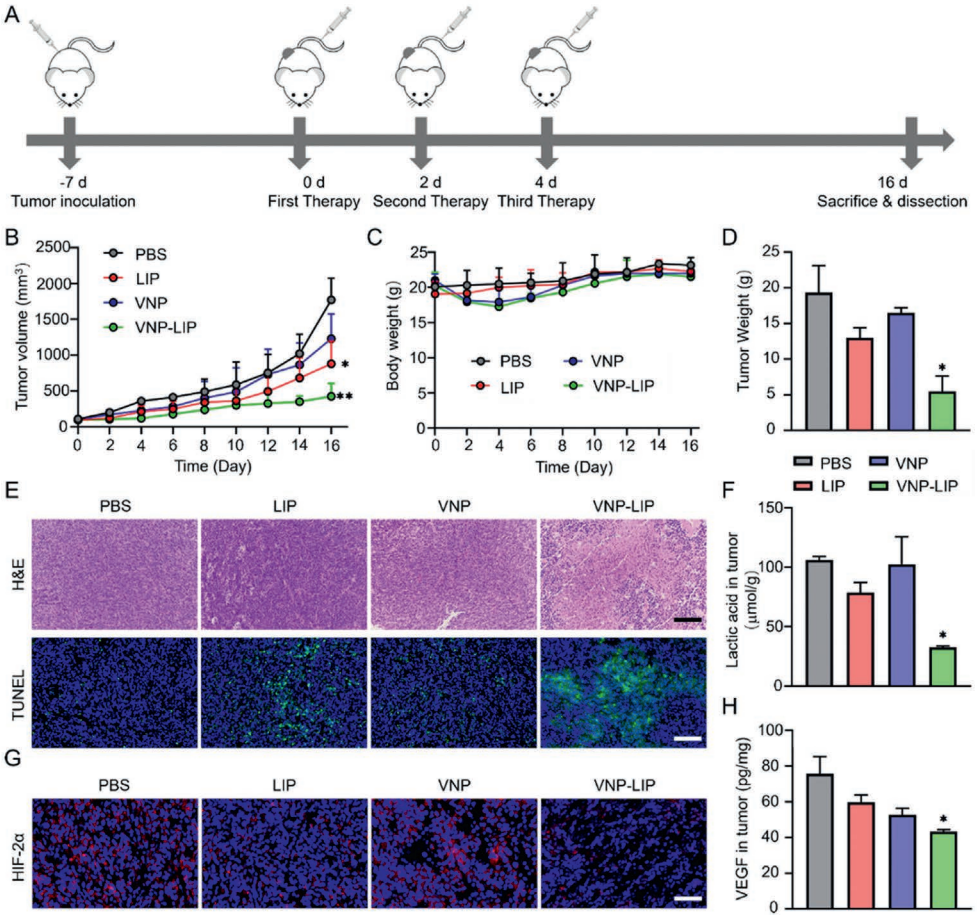


Fig. 4. (A) Schematic illustration of the *in vivo* tumor treatment process. (B) Tumor growth curves of mice with different treatments. $n = 6$. (C) Body weight of mice after various treatments. $n = 6$. (D) Tumor weight after different treatments. $n = 6$. (E) H&E and TUNEL staining of tumor sections collected from mice after different treatments. Scale bar = 100 μm (H&E staining), 50 μm (TUNEL staining). (F) Lactic acid concentration in tumor tissues after different treatments. $n = 3$. (G) Immunofluorescence staining of DAPI (blue) and HIF-2α (red) in tumor tissues after different treatments. Scale bar = 50 μm. (H) The VEGF levels of tumor tissues after different treatments. $n = 3$. Data were presented as mean ± SD. Statistical analysis was conducted using One-Way ANOVA. $^{*}P \leq 0.05$, $^{**}P \leq 0.01$, and $^{***}P \leq 0.001$.

vascularization (Fig. 4H). These results confirmed the promising therapeutic effect of VNP-LIP by targeting tumor accumulation and cyclic catalytic reaction-leading lactic acid metabolic therapy.

In summary, we have successfully designed a supramolecularly engineered bacterial reactor that performs cyclic, sustainable lactic acid consumption, for targeted metabolic cancer therapy. This innovative bioreactor is constructed through the supramolecular conjugation between cucurbit[7]uril (CB[7])-modified VNP20009 (VNP) and adamantane (ADA)-modified LOX-loaded liposomes (LIP), leveraging strong host-guest interactions. The resulting VNP-LIP system exhibits exceptional tumor targeting and accumulation, driven by the inherent tumor tropism of VNP. Once localized at the tumor sites, the catalase-like activity of VNP were stimulated by excess hydrogen peroxide (H_2O_2) in the tumor into oxygen (O_2), consuming H_2O_2 in the process. The generated O_2 is further supplied to the LOX within the liposomes to catalyze the conversion of lactic acid in the tumor microenvironment (TME) into pyruvate and hydrogen peroxide (H_2O_2), creating a continuous VNP-LOX catalytic cycle. This cycle effectively depletes lactic acid, limiting the expression of hypoxia-inducible factor 2α (HIF-2α) and reducing the production of the pro-tumoral factor vascular endothelial growth factor (VEGF). Consequently, this process inhibits tumor vascularization and growth.

On the one hand, supramolecular engineering technology could enable same-day personalized treatments. The construction of the bacterial drug delivery system can be completed by mixing the CB[7]-modified VNP and ADA-modified LOX-loaded LIP only for 3 min. Benefiting from the rapid and excellent tumor targeting effect of the VNP *in vivo*, the system can accumulate at the tumor site within two hours and reach the highest accumulation at 48 h, which is enough for the system to reach stably reflecting the potential clinical feasibility of this novel treatment.

On the other hand, the supramolecular integration of VNP and lactic acid-modulating LIP into a catalytic cyclic reactor demonstrates a promising approach to remodel the pathological microenvironment. By enhancing lactic acid catabolism, this system offers significant potential for *in vivo* anticancer applications. Our findings suggest that this bioreactor could serve as a promising strategy for targeted metabolic therapy, paving the way for novel treatments that leverage the unique properties of bacterial systems and supramolecular chemistry to combat cancer.

Declaration of competing interest

The authors declare that they have no known competing financial interests or personal relationships that could have appeared to influence the work reported in this paper.

CRediT authorship contribution statement

Xun Xu: Data curation, Conceptualization. **Jianwen Wei:** Writing – original draft, Data curation, Conceptualization. **Yuan-Fu**

Ding: Writing – review & editing, Writing – original draft, Methodology, Investigation. **Junyan Li:** Methodology. **Mian Tang:** Investigation. **Chun Wang:** Methodology. **Beibei Xie:** Methodology. **Qingwen Zhang:** Visualization, Supervision. **Yan Gao:** Supervision, Conceptualization.

Acknowledgments

This work was supported by Jiangxi Provincial Natural Science Foundation (No. 20252BAC200030), Early-Career Young Scientists and Technologists Project of Jiangxi Province (No. 20252BEJ730260), The Science and Technology Development Fund, Macau SAR (Nos. 0001/2023/RIA1, 0070/2023/RIA2 and 007/2024/STT). All animal procedures were approved by the Animal Ethics Committee, University of Macau, and the ethics approval number is UMARE-012–2024.

Supplementary materials

Supplementary material associated with this article can be found, in the online version, at doi:10.1016/j.cclet.2025.112105.

References

[1] B. Ruffell, L.M. Coussens, Cancer Cell 27 (2015) 462–472.
[2] D.F. Quail, J.A. Joyce, Nat. Med. 19 (2013) 1423–1437.
[3] S. Li, H. Yue, S. Wang, et al., Adv. Drug Deliv. Rev. 188 (2022) 114444.
[4] P. Vaupel, G. Multhoff, J. Physiol. 599 (2021) 1745–1757.
[5] U.E. Martinez-Outschoorn, M. Peiris-Pagés, R.G. Pestell, F. Sotgia, M.P. Lisanti, Nat. Rev. Clin. Oncol. 14 (2017) 11–31.
[6] C. Wei, C. Yang, S. Wang, et al., Mol. Cancer 18 (2019) 1–23.
[7] S. Sun, H. Li, J. Chen, Q. Qian, Physiology 32 (2017) 453–463.
[8] C. Hayes, C.L. Donohoe, M. Davern, N.E. Donlon, Cancer Lett. 500 (2021) 75–86.
[9] Q. Cheng, X.L. Shi, Q.L. Li, L. Wang, Z. Wang, Adv. Sci. 11 (2024) 2305662.
[10] S. Zhao, J. Hou, L. Deng, et al., Angew. Chem. Int. Ed. 64 (2025) e20242220.
[11] N. Liu, J. Luo, D. Kuang, et al., J. Clin. Invest. 129 (2019) 631–646.
[12] L. Hou, Y. Zhao, G.Q. Song, et al., Cancer Cell Int. 19 (2019) 1–12.
[13] G.H. Mohammad, V. Vassileva, P. Acedo, et al., Cancers 11 (2019) 1372.
[14] M. Beloueche-Babari, S. Wantuch, T.C. Galobart, et al., Cancer Res. 77 (2017) 5913–5924.
[15] Z.X. Liao, I.M. Kempson, C.C. Hsieh, S.J. Tseng, P.C. Yang, Drug Discov. Today 26 (2021) 2508–2514.
[16] F. Alam, S. RoyChoudhury, A.H. Jalal, et al., Biosens. Bioelectron. 117 (2018) 818–829.
[17] Z. Tian, K. Yang, T. Yao, et al., Small 15 (2019) 1–8.
[18] J. Tang, A.K. Meka, S. Theivendran, et al., Angew. Chem. Int. Ed. 59 (2020) 22054–22062.
[19] X. Zhou, W. Zhao, M. Wang, et al., ACS Appl. Mater. Interfaces 12 (2020) 32278–32288.
[20] Z. Zhang, B. Li, L. Xie, et al., ACS Nano 15 (2021) 16934–16945.
[21] F. Gao, Y. Tang, W.L. Liu, et al., Adv. Mater. 31 (2019) 1–13.
[22] H. Wang, X. Huang, R. Gao, et al., ACS Appl. Mater. Interfaces 17 (2025) 7275–7290.
[23] J. Chen, Y. Zhu, C. Wu, J. Shi, Chem. Soc. Rev. 52 (2023) 973–1000.
[24] S.C. Liu, N.P. Minton, A.J. Giaccia, J.M. Brown, Gene Ther. 9 (2002) 291–296.
[25] Y.A. Yu, S. Shabahang, T.M. Timiryasova, et al., Nat. Biotechnol. 22 (2004) 313–320.
[26] K.M. Broadway, S. Suh, B. Behkam, B.E. Scharf, J. Biotechnol. 251 (2017) 76–83.
[27] J.F. Toso, V.J. Gill, P. Hwu, et al., J. Clin. Oncol. 20 (2002) 142–152.
[28] M.R. Charbonneau, V.M. Isabella, N. Li, C.B. Kurtz, Nat. Commun. 11 (2020) 1–11.
[29] T. Yin, Z. Diao, N.T. Blum, et al., Small 18 (2022) 1–14.
[30] C.H. Lee, C.L. Wu, A.L. Shiau, Int. J. Cancer 122 (2008) 930–935.
[31] D.M. Wall, C.V. Srikanth, B.A. McCormick, Oncotarget 1 (2010) 721–728.
[32] C. Clairmont, K.C. Lee, J. Pike, et al., J. Infect. Dis. 181 (2000) 1996–2002.
[33] B. Ezraty, A. Gennaris, F. Barras, J.F. Collet, Nat. Rev. Microbiol. 15 (2017) 385–396.
[34] C.C. Winterbourn, A.J. Kettle, Antioxid. Redox Signal. 18 (2013) 642–660.
[35] M.F. Christman, R.W. Morgan, F.S. Jacobson, B.N. Ames, Cell 41 (1985) 753–762.
[36] M.F. Christman, G. Storz, B.N. Ames, Proc. Natl. Acad. Sci. U. S. A. 86 (1989) 3484–3488.
[37] F. Wu, J. Liu, Adv. Drug Deliv. Rev. 188 (2022) 114443.
[38] Y. Ma, S. Yan, X. Xu, H. Cao, R. Wang, Chin. Chem. Lett. 35 (2024) 108645.
[39] J.H. Tian, H. Xu, X.Y. Hu, D.S. Guo, Supramol. Mater. 3 (2024) 100063.
[40] J.J. Chu, R. Mehrzad, Link Between Obes. Cancer 38 (1974) 23–34.
[41] C. Gao, Q. Cheng, J. Li, et al., Adv. Funct. Mater. 31 (2021) 2102440.
[42] L.B. Ivashkiv, Nat. Rev. Immunol. 20 (2020) 85–86.
[43] Q. Chen, H. Bai, W. Wu, et al., Nano Lett. 20 (2020) 11–21.
[44] T. Yamamoto, Y. Teramura, T. Itagaki, Y. Arima, H. Iwata, Sci. Technol. Adv. Mater. 17 (2016) 677–684.
[45] T.K. Korhonen, K. Lounatmaa, H. Ranta, N. Kuusi, J. Bacteriol. 144 (1980) 800–805.
[46] N. Agrawal, C. Bettegowda, I. Cheong, et al., Proc. Natl. Acad. Sci. U. S. A. 101 (2004) 15172–15177.
[47] S. Zhou, C. Gravekamp, D. Bermudes, K. Liu, Nat. Rev. Cancer 18 (2018) 727–743.
[48] C. Gao, C. Liu, Q. Chen, et al., J. Control Release 349 (2022) 2–15.